5

Photometry and astrometry

One of the basic astronomical pursuits throughout history has been to determine the amount and temporal nature of the flux emitted by an object as a function of wavelength. This process, termed photometry, forms one of the fundamental branches of astronomy. Photometry is important for all types of objects from planets to stars to galaxies, each with their own intricacies, procedures, and problems. At times, we may be interested in only a single measurement of the flux of some object, while at other times we could want to obtain temporal measurements on time scales from seconds or less to years or longer. Some photometric output products, such as differential photometry, require fewer additional steps, whereas to obtain the absolute flux for an object, additional CCD frames of photometric standards are needed. These standard star frames are used to correct for the Earth's atmosphere, color terms, and other possible sources of extinction that may be peculiar to a given observing site or a certain time of year (Pecker, 1970).

We start this chapter with a brief discussion of the basic methods of performing photometry when using digital data from 2-D arrays. It will be assumed here that the CCD images being operated on have already been reduced and calibrated as described in detail in the previous chapter. We will see that photometric measurements require that we accomplish only a few steps to provide output flux values. Additional steps are then required to produce light curves or absolute fluxes. Remember, for a photometrist, every photon counts but the trick is to count every photon.

As an introduction to the level of atmospheric extinction one might expect as a function of observational elevation and wavelength, Table 5.1 lists values of the extinction in magnitudes resulting from the Earth's atmosphere for an observing site at 2200 m elevation. Note that for observations made at reasonable airmass and redward of 4000 Å, the effect of the Earth's atmosphere is, at worst, a few tenths of a magnitude. The details of photometric corrections

https://doi.org/10.1017/CBO9780511807909.007

Table 5.1. *Example Atmospheric Extinction Values (Magnitudes)*

Altitude	Airmass	3000 Å	3500 Å	4000 Å	4500 Å	5000 Å	5500 Å	6000 Å	6500 Å	7000 Å	8000 Å	9000 Å	10 000 Å
90	1.00	1.2	0.65	0.4	0.3	0.2	0.2	0.2	0.1	0.1	0.1	0.1	0.1
75	1.04	1.2	0.65	0.4	0.3	0.2	0.2	0.2	0.1	0.1	0.1	0.1	0.1
60	1.15	1.3	0.75	0.5	0.3	0.3	0.2	0.2	0.2	0.1	0.1	0.1	0.1
45	1.41	1.6	0.9	0.6	0.4	0.3	0.3	0.2	0.2	0.2	0.1	0.1	0.1
30	1.99	2.3	1.3	0.8	0.6	0.4	0.4	0.3	0.3	0.2	0.2	0.1	0.1
20	2.90	3.3	1.55	1.2	0.8	0.6	0.5	0.5	0.4	0.3	0.2	0.2	0.2
15	3.82	4.4	2.5	1.6	1.1	0.8	0.7	0.6	0.5	0.4	0.3	0.3	0.2
10	5.60	6.4	3.65	2.3	1.6	1.2	1.1	1.0	0.7	0.6	0.4	0.4	0.3
5	10.21	11.8	6.7	4.2	2.9	2.2	1.9	1.7	1.4	1.1	0.8	0.7	0.6

for the Earth's atmosphere and extinction effects are not germane to the topic of this book and their discussion here would be beyond the allowed space limitations. The interested reader is referred to the excellent presentations in Young (1974), Hendon & Kaitchuck (1982), Dacosta (1992), and Romanishin (2004). Further good discussions of photometric data handling are presented in Hiltner (1962), Howell & Jacoby (1986), Stetson (1987), Walker (1990), Howell (1992), Merline & Howell (1995), and Howell, Everett, & Ousley (1999).

5.1 Stellar photometry from digital images

Prior to the time when CCDs became generally available to the astronomical community, digital images of astronomical objects were being produced by detectors such as silicon intensified targets (SITs), video tube-type cameras, image tubes, and electronographic cameras. In addition, scanning of photographic plates with a microdensitometer resulted in large amounts of digital output. These mechanisms produced digital data in quantity and at rates far in excess of the ability of workers to individually examine each object of interest within each image. Today, the amount of CCD data greatly exceeds this limit. Thus, in the early 1980s, work began in earnest to develop methods by which photometry could be obtained from digital images in a robust, mostly automated manner.

One of the first such software packages to deal with digital images was written by Adams, Christian, Mould, Stryker, and Tody (Adams *et al.*, 1980) in 1980. Numerous other papers and guides have been produced over the years containing methods, ideas, entire software packages that perform photometry, and specific detailed information for certain types of objects. I have tried to collect a fairly complete list of these in Appendix A. While details vary, the basic photometric toolbox must contain methods that perform at least the following primary tasks: (i) image centering, (ii) estimation of the background (sky) level, and (iii) calculation of the flux contained within the object of interest. We will assume below, for simplicity, that we are working with stellar images that to a good approximation are well represented by a point-spread function of more-or-less Gaussian shape. Deviations from this idealistic assumption and nonpoint source photometry will be discussed as they arise.

5.1.1 Image centering

Probably the simplest and most widely used centering approximation for a point-spread function (PSF) is that of marginal sums or first moment distributions. Starting with a rough pointer to the position of the center of the star (e.g., the cursor position, reading off the x, y coordinates, or even a good guess), the intensity values of each pixel within a small box centered on the image and of size $2L+1 \times 2L+1$ (where L is comparable to the size of the PSF) are summed in both x and y directions (see Figure 5.1). The x, y center is computed as follows: the marginal distributions of the PSF are found from

$$I_i = \sum_{j=-L}^{j=L} I_{i,j}$$

and

$$J_j = \sum_{i=-L}^{i=L} I_{i,j},$$

where $I_{i,j}$ is the intensity (in ADU) at each x, y pixel; the mean intensities are determined from

$$\bar{I} = \frac{1}{2L+1} \sum_{i=-L}^{i=L} I_i$$

and

$$\bar{J} = \frac{1}{2L+1} \sum_{j=-L}^{j=L} J_j;$$

and finally the intensity weighted centroid is determined using

$$x_c = \frac{\Sigma_{i=-L}^{i=L}(I_i - \bar{I})x_i}{\Sigma_{i=-L}^{i=L}(I_i - \bar{I})}$$

for all $I_i - \bar{I} > 0$ and

$$y_c = \frac{\Sigma_{j=-L}^{j=L}(J_j - \bar{J})y_j}{\Sigma_{j=-L}^{j=L}(J_j - \bar{J})}$$

for all $J_j - \bar{J} > 0$.

For well-sampled (see Section 5.9), relatively good S/N (see Section 4.4) images, simple x, y centroiding provides a very good determination of the center position of a PSF, possibly as good as one fifth of a pixel. More sophisticated schemes to provide better estimations of image centers or applications appropriate to various types of non-Gaussian PSFs are given in Chiu (1977), Penny & Dickens (1986), Stone (1989), Lasker *et al.* (1990b), Massey & Davis (1992), Davis (1994), and Howell *et al.* (1996).

5.1.2 Estimation of background

The importance of properly estimating the background level on a CCD resides in the fact that the same pixels that collect photons of interest from an astronomical source also collect photons from the "sky" or background, which

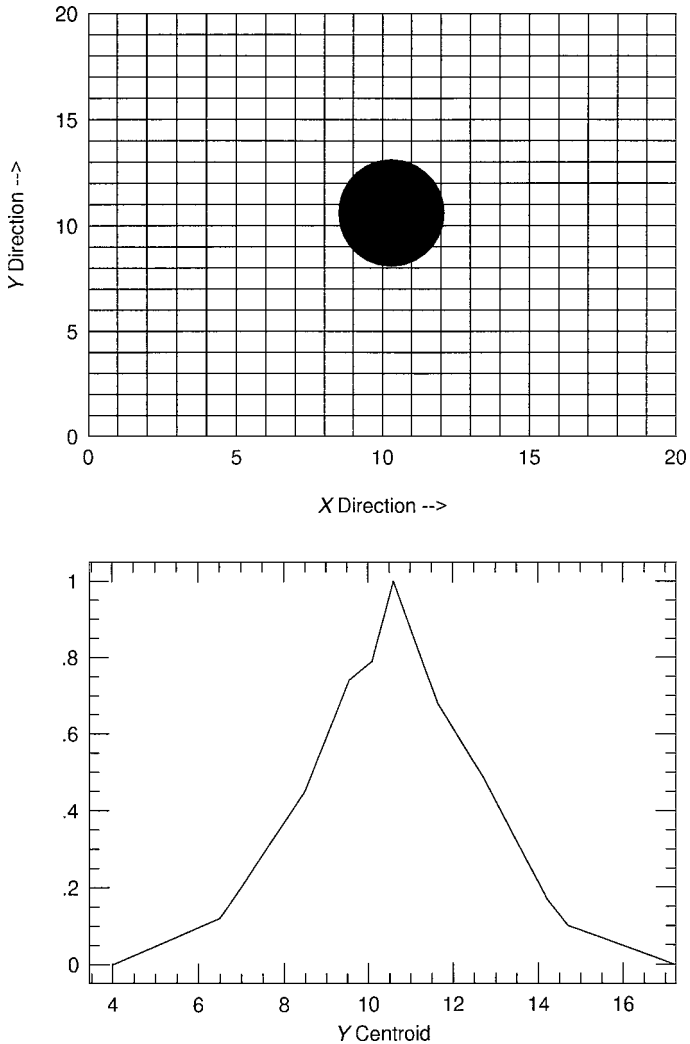

Fig. 5.1. An example of x, y centroiding. The idealized star image in the top box sits on a pixel grid with a center of $(x, y) = (10.3, 10.6)$. The two other plots represent the x, y centroids for the star image normalized to a maximum height of one. In this case, the star center is well approximated by the peaks in the x, y centroids.

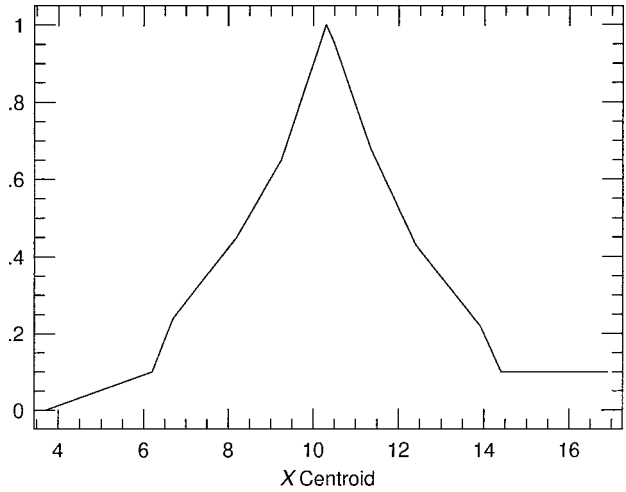

Fig. 5.1. (cont.)

are of no interest. Remember that the background or sky value in a CCD image contains not only actual photons from the sky but also photons from unresolved astronomical objects, read noise, thermally generated dark current electrons, and other sources. All of these unwanted additional photons must be accounted for in some manner, estimated, and removed from the image before a final determination of the source flux is made. In order to determine this background level, a common technique is to place a software annulus around the source of interest and then use statistical analysis to estimate its mean level on a per pixel basis.

The background or sky annulus is usually defined by an inner and outer radius or by an inner radius and a width (see Figure 5.2). One simple, yet powerful, manner by which an estimation of the background level can be made is simply to extract the values of all the pixels within the annulus, sum them, and divide by the total number of pixels within the annulus. This provides an average value per pixel for the background level of the CCD image. For a good statistical determination of the background level, the total number of pixels contained within this annulus should be relatively large, about three times the number contained within that of the source aperture (Merline & Howell, 1995).[1] A more robust estimator, requiring very little

[1] Partial pixels arising from placing a circular annulus on a rectangular grid are usually not of concern here, as the number of annulus pixels is large. However, partial pixels cannot be so easily dismissed when we are determining the intensity within the much smaller source aperture.

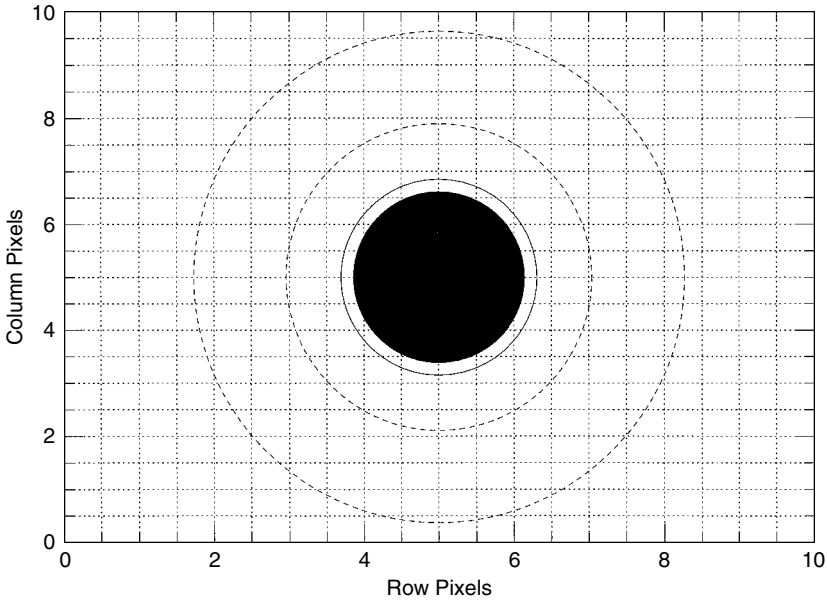

Fig. 5.2. Schematic drawing of a stellar image on a CCD pixel grid. The figure shows the location of the star, the "star" aperture (solid line), and the inner and outer "sky" annuli (dashed circles).

additional work, is to collect all the pixel values from inside the sky annulus, order them in increasing value, and find the median intensity, B_M.[1] A nice touch here is to reexamine the list of annulus pixel values and toss out all those with values greater than $\pm 3\sigma$ from B_M. This last step will eliminate cosmic ray hits, bad pixels, and contamination from close-by astronomical neighbors if they exist.

When applying a median filter and the 3σ cutoff technique to the list of background pixels, one can use the remaining annulus pixel values to construct a background histogram computed with a bin width resolution of say 0.5 ADU (Figure 5.3). The background histogram will be centered on the median background value with all contained pixel values within $\pm 3\sigma$. Since the detailed resolution of 0.5 ADU binning will likely produce a ragged histogram (since only a finite number of background pixels is used), some smoothing of the histogram may be useful, such as that done by Lucy (1975).

[1] Note that the statistical values determined from a CCD image for the median or the mode must pick their answer from the list of the actual CCD pixel ADU values, that is, values that are integers containing only digitized levels and thus digitization noise. The statistical mean, however, allows for noninteger answers. This seemingly subtle comment is of great importance when dealing with partial pixels, undersampled data, or high CCD gain values.

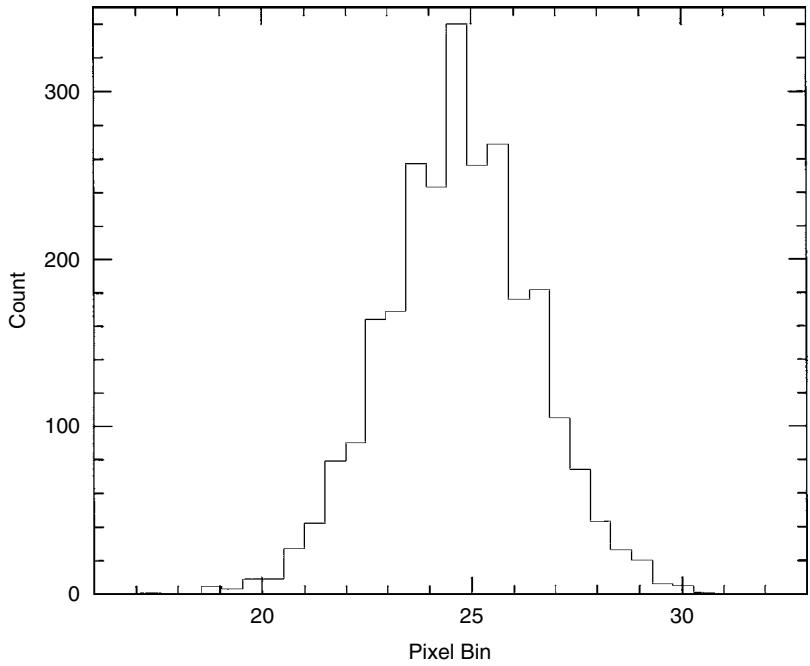

Fig. 5.3. Histogram of the "sky" annulus around a star in the CCD image shown in Figure 4.5. Notice the roughly Gaussian shape to the sky distribution but with an extended tail toward larger values. This tail is due to pixels that were not completely calibrated in the reduction process, pixels with possible contamination due to dark current or cosmic rays, pixels with increased counts due to unresolved PSF wings from nearby stars, and contamination of sky annulus pixels by faint unresolved background objects. The need for some histogram smoothing, such as that described in the text, is apparent, especially near the peak of the distribution.

Lucy smoothing will broaden the histogram distribution slightly after one iteration but application of a second iteration will restore the correct shape and provide a smooth histogram from which to proceed. This final step produces a statistically valid and robust estimator from which we can now compute the mean value of the background, $\bar{B}$. A determination of the centroid of the final smoothed histogram, using equational forms for the centroid in one dimension such as those discussed above, can now be applied. Centroiding of this smoothed histogram is not influenced by asymmetries that may have been present in the wings of the initially unsmoothed values.

Correct estimation of the level of the CCD background on a per pixel basis is of increasing importance as the S/N of the data decreases and/or the CCD pixel sampling becomes poor. A background level estimation for each pixel

that is off by as little as a few ADU can have large effects on the final result (Howell, 1989). Determination of the CCD background level has an associated error term $\propto (1 + n_{\rm pix}/n_B)^{-1/2}$, which should be included in the S/N calculation of the final result. The "sky" is the limit.

5.1.3 Estimation of point source intensity

We now come to the pixel values of interest, that is, those that contain photons from the source itself. Using a software aperture of radius r centered on the x, y position of the centroid of the source PSF, we can extract the values from all pixels within the area $A(= \pi r^2)$ and sum them to form the quantity S, the total integrated photometric source signal. The sum S contains contributions from the source but also from the underlying background sources within A. To remove the estimated contribution to S from the background, we can make use of the value $\bar{B}$, discussed above. We can calculate an estimate of the collected source intensity, I, as $I = S - n_{\rm pix}\bar{B}$, where $n_{\rm pix}$ is the total number of pixels contained within the area A. There are some additional minor considerations concerning this procedure but these will not be discussed here (Merline & Howell, 1995).

A final step usually performed on the quantity I, which we will discuss further below, is to determine a source magnitude. The value of a magnitude is defined by the following standard equation:

$$\text{Magnitude} = -2.5 \log_{10}(I) + C,$$

where I is the source intensity per unit time, that is, the flux (universally given as per second), and C is an appropriate constant (usually $\sim$23.5–26 for most earthly observing sites) and determined in such a manner so that the calculated source magnitude is placed on a standard magnitude scale such as that of the Johnson system or the Strömgren system.

As we mentioned above, when using circular apertures on rectangular pixel grids, partial pixels are inevitable. While we could toss them away for the large background area, we cannot follow a similar sloppy procedure for the smaller source aperture. Thus the question becomes, how do we handle partial pixels? This is not a simple question to answer and each photometric software package has its own methodology and approach. The three choices a software package can use are:

1. Do not use partial pixels at all. Any source intensity that falls into the source aperture but within a partially inscribed pixel is simply not used in the calculation of S.

2. Sum the values for every pixel within the source aperture regardless of how much or how little of the pixel area actually lies within A.
3. Make use of some computational weighting scheme that decides, in a predefined manner, how to deal with the counts contained within each partial pixel in the source aperture.

This last choice often uses the ratio of the pixel area inside the source aperture to that outside the aperture as a simple weighting factor. A computational scheme to handle partial pixels in a software package designed to perform digital photometry is the hardest of the above choices to implement, but it will provide the best overall final results. To know exactly how a certain software package handles partial pixels, the user is referred to the details presented within the documentation provided with the software. Many PC-type packages that perform photometry on CCD images do not detail their partial pixel and magnitude calculation methods and are therefore "black boxes" to be avoided.

There are two basic methods by which most observers estimate the total integrated signal within their source aperture: point-spread function fitting and digital aperture photometry. The first method relies on fitting a 2-D function to the observed PSF and using the integrated value underneath this fitted function as an estimate of S. The second method, digital aperture photometry, attempts to place a software aperture about the source profile (as shown in Figure 5.2), centered in some manner (e.g., x, y centroids), and then simply sums the pixel values within the source aperture to provide the estimation of S. We will discuss each of these methods in turn below and note here that it is unlikely that a single method of estimation will be the best to use in all possible situations. For example, for severely undersampled data the method of pixel mask fitting (Howell *et al.*, 1996) provides the best solution.

5.2 Two-dimensional profile fitting

The profiles of astronomical point sources that are imaged on two-dimensional arrays are commonly referred to as point-spread functions or PSFs. In order to perform measurements on such images, one method of attack is profile fitting. PSFs can be modeled by a number of mathematical functions, the most common include Gaussian,

$$G(r) \propto \mathrm{e}^{\left(\frac{r^2}{2a^2}\right)},$$

modified Lorentzian,

$$L(r) \propto \frac{1}{1+(r^2/a^2)^b},$$

https://doi.org/10.1017/CBO9780511807909.007

and Moffat,

$$M(r) \propto \frac{1}{(1 + r^2/a^2)^b}$$

representations, where r is the distance from the center of the point source and a and b are fitting parameters (Stetson, Davis, & Crabtree, 1990). These types of functional forms can be used to define the PSF for each star within an image by the assumption that they provide a good representation of the data themselves. For example, adjustment of the values of a and b within one of these functions may allow an imaged PSF to be matched well in radius and profile shape (height and width), allowing a simple integration to be performed to measure the underlying flux.

Generally, the above functions are only a fair match to actual PSFs and so a second method of profile fitting can be applied. This method consists of using an empirical PSF fit to the actual digital data themselves, producing modified versions of the above functions. Depending on the application, PSFs may be evaluated at the center of a pixel or integrated over the area of each pixel. Even more general methods of allowing the data to produce completely analytic forms for the PSF functions have been attempted. The techniques and use of empirical PSFs could fill an entire chapter; we refer the reader to King (1971), Diego (1985), and Stetson (1987) for more details.

Both techniques, the use of completely mathematical forms for a PSF approximation and the more empirical method, have their advantages and disadvantages. Model PSF fitting allows the necessary integrations and pixel interpolations to be carried out easily as the functions are well known, while the empirical method, which makes hardly any assumptions about the actual shape of the PSF, is only defined on the CCD pixel grid and not in any general mathematical way. This latter complication can cause difficulties when trying to interpolate the empirical shape of one PSF somewhere on the CCD (say a bright reference star) to a PSF located somewhere else on the same image but that is likely to have a different pixel registration. For this reason, some implementations of empirical PSF fitting actually make use of the sum of an analytic function (such as one of those given as above) and a look-up table of residuals between the actual PSF and the fitting function. Figure 5.4 shows examples of some PSF models and some actual PSFs obtained with CCDs.

Procedurally, profile fitting techniques work by matching the implied PSF to the actual digital data in a 2-D fashion and within some radius, r, called the fitting radius. An attempt is then made to maximize some goodness-of-fit criteria between the assumed PSF and the observed one. PSF fitting can be further optimized by fitting N point sources within the image simultaneously

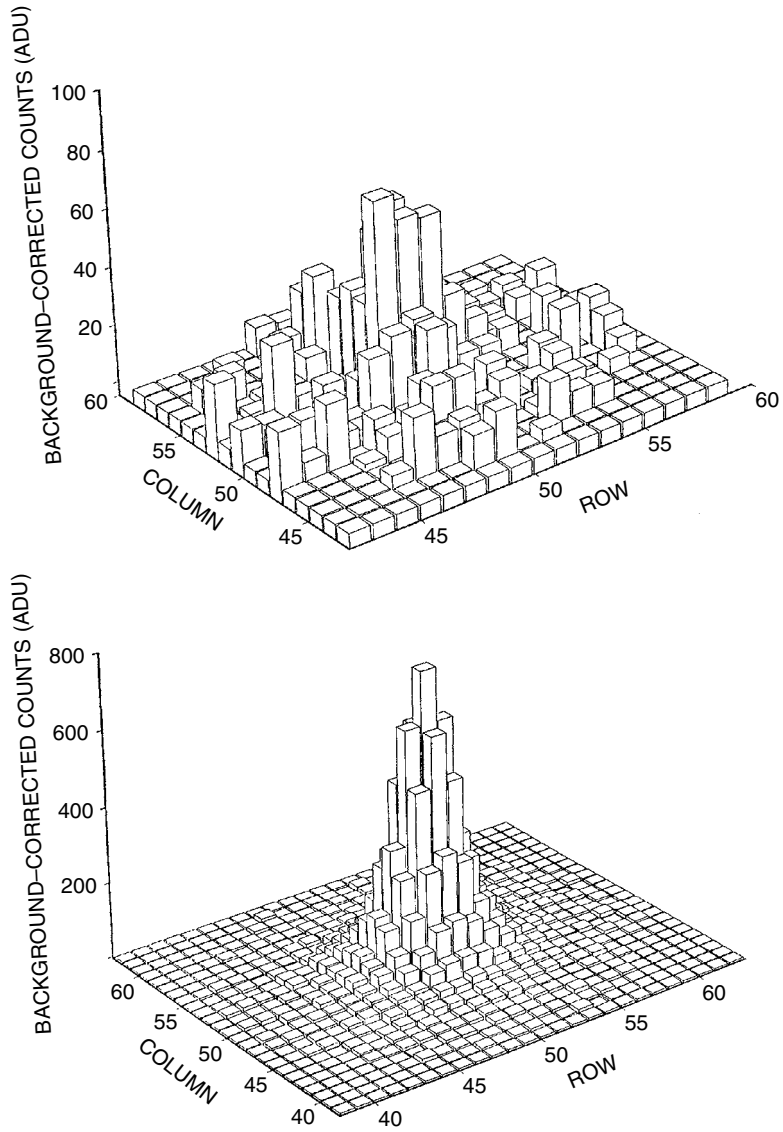

Fig. 5.4. Stellar PSFs are shown for various cases. The figure above shows two model PSFs, one for a bright star (S/N ∼125) and one for a faint star (S/N ∼20). The remaining two panels show similar brightness stars but are actual CCD data. Note that the models are shown as 3-D pixel histograms whereas the real data are represented as spline profile fits to the actual PSFs. The disadvantage of the latter type of plotting is that the true pixel nature of the image is lost.

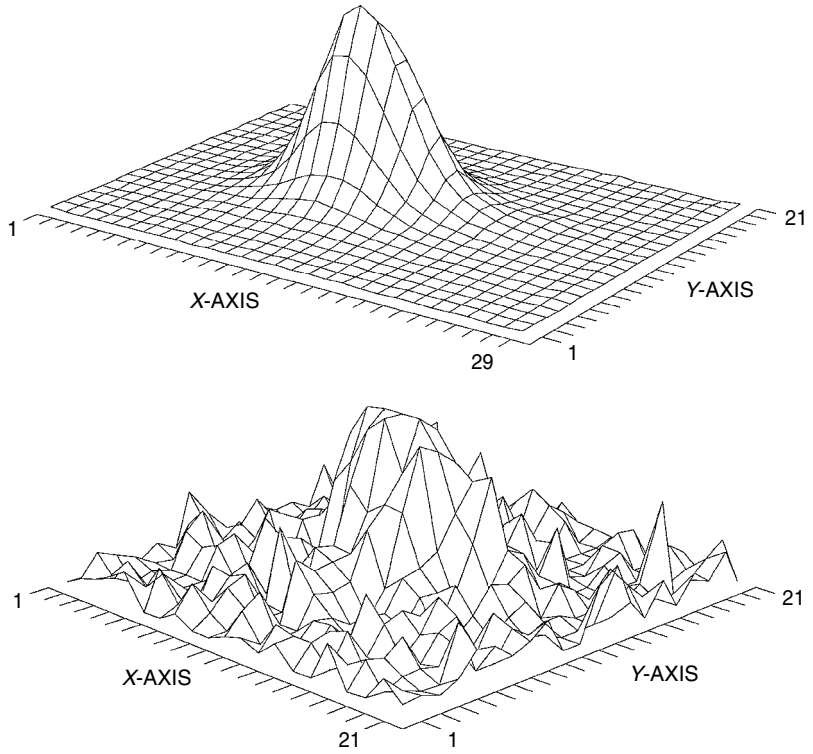

Fig. 5.4. (cont.)

(usually one uses the brightest stars within the image) and using some combination of statistically weighted mean values for the final fitting parameters. PSF fitting can be very computationally demanding, much more so than the method of aperture photometry discussed below. However, for some types of imagery, for example crowded fields such as within star clusters for which some PSFs may overlap, PSF fitting may be the only method capable of producing scientifically valid results (Stetson, 1987, 1992, 1995).

5.3 Difference image photometry

One method used today for studies of photometric variability is the technique of difference image photometry (DIA), also called difference image analysis or image subtraction (Tomaney & Crotts, 1996). DIA is useful in (very) crowded field photometry or when searching for variable sources that may be blended with other possibly nonpoint sources. Most modern photometric searches for supernovae in external galaxies or gravitational lenses use DIA

as these studies involve imaging in very crowded stellar fields and searching for highly blended sources.

The basic idea of DIA is to take a reference image and subtract from it images of the same field of view but taken at different times. An example would be to take a CCD image of a star cluster at an airmass of one and use this as your reference image. Additional images taken of this same field over time are then each subtracted from the reference image and variable sources show up in the difference image. Figure 5.5 shows a nice example of DIA from the supermacho project being carried out at the CTIO 4-m telescope in Chile. The reference image may actually be a sum of some number of the best images obtained (say during the best seeing) or an image observed at the lowest airmass. In practice, DIA is not so simple and involves setting up a CPU intensive, fairly complex software pipeline.

Before the simple process of subtraction from the reference image can occur, each successive image must be positionally registered, photometric normalized, and adjusted for other offending effects such as differential refraction, seeing and telescope focus changes, and possibly sky conditions. The matching of the point-spread functions between frames can be accomplished by Fourier divison (Alcock *et al.*, 1999) or a linear kernal decomposition in real space (Alard, 2000). Right away one can see that this is not a simple process. It involves setting up various transformation processes in software and a diligent eye to make sure they all work correctly in an automated

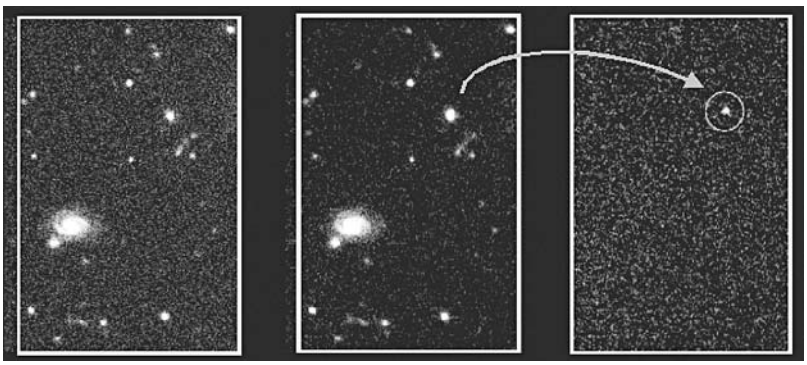

Fig. 5.5. An example of difference image analysis. The image was produced by C. Stubbs as a part of the high-z supernovae team using the supermacho data set. The image on the left is the reference image taken at epoch 1, the middle image is from epoch 2, 3 weeks later, and the right image is their difference. A supernova blended with its host galaxy image (middle frame) is clearly detected in the difference image.

fashion. Errors in these flux manipulation steps can be large and are often unaccounted for in the final result.

DIA is somewhat akin to profile fitting but is done on a frame-by-frame basis. The two-dimensional profile of each object in one frame is transformed to match those of the reference frame. One can model the profiles in a given frame using some small fraction of the brightest uncrowded sources per frame and applying the same model mapping of these sources to the reference frame to all objects in the given frame (Alcock *et al.*, 1999). This procedure saves CPU time but may introduce some uncertainty as it relies on a few of the brightest sources to be an exact match to the remaining sources. Spatial dependence, color dependence, pixel sampling, and seeing can all vary across an image and are hard to correct for perfectly. DIA has been used very effectively in a number of projects and continues to be the method of choice in certain regimes where crowding of some fashion is prevalent. The accuracy of the photometry delivered depends on how well the software processes of registration, convolution, and normalization are performed and what assumptions are used. For example, some DIA analysis assumes that stellar colors are well approximated by blackbody functions and in other cases that the bright stars well represent the remaining (fainter) stars. Both of these assumptions are valid to a point but are highly efficient in terms of processing the data. To date, photometric differences of 0.5 magnitude or better are easy to detect in a single difference frame. Thus DIA is a good technique for finding fairly large amplitude changes (i.e., newly brightened sources) but its ability to produce highly accurate light curves is yet to be fully explored.

The process of DIA is a mixture of photometry and astrometry plus profile fitting and using software to remap images to match the reference image. If observations are obtained of fields of interest that are not crowded or blended, than DIA is overkill and profile fitting or differential photometry (see below) work well and are easier to implement. These latter two techniques are also not subject to the addition of photon noise via the difference processing or any additional systematic effects as exist in DIA. But, as we note, every photometric technique has pros and cons and for highly blended or crowded fields DIA is a useful tool (see Tomaney & Crotts, 1996, Zebrun *et al.*, 2001, and references therein).

5.4 Aperture photometry

Aperture photometry is a technique that makes no assumption about the actual shape of the source PSF but simply collects and sums up the observed counts within a specified aperture centered on the source. The aperture used may be

circular (usually the case for point sources), square, or any shape deemed useful. Aperture photometry is a simple technique, both computationally and conceptually, but this same simplicity may lead to errors if applied in an unsuitable manner or when profile fitting is more appropriate (e.g., severe blending).

The basic application of aperture photometry starts with an estimate of the center of the PSF and then inscribes a circular software aperture of radius r about that center. The radius r may simply be taken as three times the full-width at half-maximum ($r = 3{\cdot}\text{FWHM}$): the radius of a PSF that would contain 100% of the flux from the object (Figure 5.6) (Merline & Howell, 1995). Summing the counts collected by the CCD for all the pixels within the area $A = \pi r^2$, and removing the estimated background sky contribution within A, one finally arrives at an estimated value for I. We see again that partial pixels (a circular software aperture placed on a rectangular grid) are an issue, even for this simple technique. Using a square or rectangular aperture alleviates the need for involving partial pixels but may not provide the best estimate of the source flux. Noncircular apertures do not provide a good match to the 2-D areal footprint of a point source, thereby increasing the value of n_{pix} that must be used and decreasing the overall S/N of the measurement. Remember, however, that for bright sources, n_{pix} is essentially of no concern (see Section 4.4).

It has been shown (Howell, 1989; Howell, 1992) that there is a well-behaved relation between the radius of the aperture of extraction of a point source and the resultant S/N obtained for such a measurement. An optimum

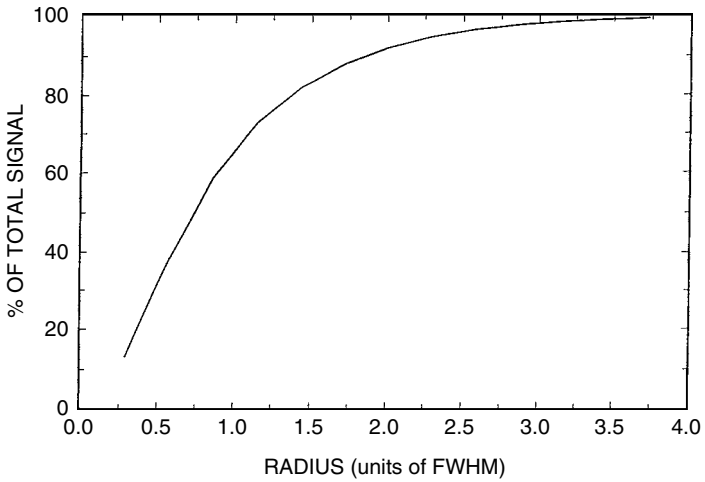

Fig. 5.6. For any reasonable PSF approximation, the figure above shows the run of the total encircled signal with radius of the PSF in FWHM units. Note that within a radius of 3·FWHM essentially 100% of the signal is included.

radius aperture, that is, one that provides the optimum or best S/N for the measurement, can be determined for any given PSF and generally has a radius of near $1 \cdot \mathrm{FWHM}$. This optimum radius is a weak function of the source brightness, becoming smaller in size for fainter sources. Figure 5.7 illustrates this idea for three point sources of different brightness.

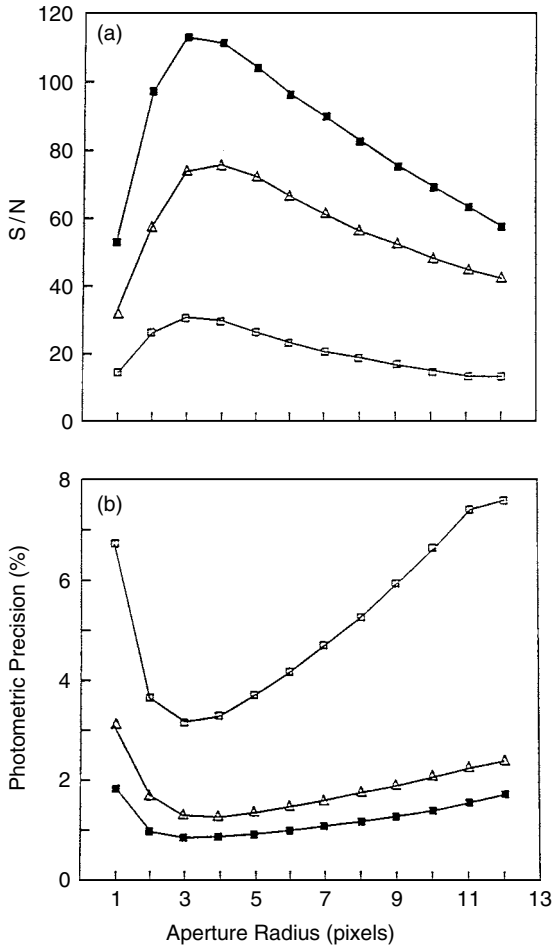

Fig. 5.7. The S/N obtained for the measurement of a point source is not constant as a function of radius. There is an optimum radius at which the S/N will be a maximum. The top panel shows this effect for three point sources that differ in brightness by 0.3 (middle curve) and 2.0 (bottom curve) magnitudes compared with the top curve (filled squares). The bottom panel presents the same three stars as a function of their photometric precision. The image scale is 0.4 arcsec/pixel and the seeing (FWHM) was near 1.2 arcsec. From Howell (1989).

To understand the idea of an optimum radius and why such a radius should exist, one simply has to examine the S/N equation given in Section 4.4 in some detail. To obtain a higher S/N for a given measurement, more signal needs to be collected. To collect more signal, one can use a larger aperture radius, up to the maximum of $3 \cdot \mathrm{FWHM}$. However, the larger r is, the more pixels that get included within the source aperture and the larger the value of n_{pix}. As n_{pix} increases, so does the contribution to the error term from noise sources other than the source itself. Thus, a balance between inclusion of more signal (larger r) and minimizing n_{pix} in the source aperture (smaller r) leads to an optimum extraction radius for a given source.

We saw in Figure 5.7 that if extracted at or very near an aperture radius of $3 \cdot \mathrm{FWHM}$, 100% of the light from a point source would be collected. However, to obtain the maximum S/N from your measurement, extraction at a smaller radius is warranted. If one extracts the source signal using an aperture that is smaller then the actual PSF radius itself, some of the source light that was collected by the CCD is not included in the summing process and is thus lost. This sounds like an incorrect methodology to use, but remember that inclusion of many pixels lying far from the source center also means inclusion of additional noise contributions to the aperture sum. Therefore, while one may wish to obtain the maximum S/N possible through the use of a smaller aperture (i.e., summation of less than the total collected source counts), for the final result it is often necessary to correct the answer obtained for this shortcoming.

In order to recover the "missing light," one can make use of the process of aperture corrections or growth curves as detailed by Howell (1989) and Stetson (1992). Growth curves do not make any demands on the underlying PSF except through the assumption that any bright stars used to define the aperture corrections are exact PSF replicas of any other (fainter) stars that are to be corrected. As we can see in Figure 5.8, growth curves for the brightest stars follow the same general shape, leading to minor or no necessary aperture corrections at a radius of $3 \cdot \mathrm{FHWM}$. The fainter stars, however, begin to deviate from the canonical growth curve at small radii, resulting in 0.5 up to 1.5 magnitudes of needed aperture correction. In general, as a point source becomes fainter, the wings of the source will contain pixels that have an increasingly larger error contribution from the background, leading to greater deviations from a master growth curve at large r, and thus a larger aperture correction will be needed.

As we will see below, if differential photometric results are desired, the aperture corrections used to bring the extracted source signal back to 100% are not necessary. This is only strictly true if all point sources of interest

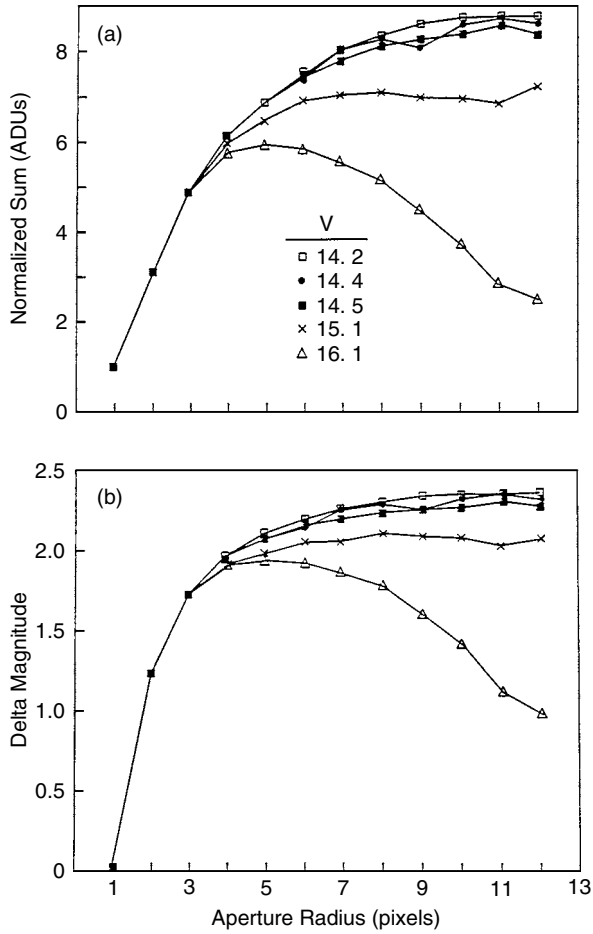

Fig. 5.8. Growth curves for five stars on a single CCD frame. The three brightest stars follow the same curve, which is very similar to the theoretical expectation as shown in Figure 5.6. The two faint stars start out in a similar manner, but eventually the background level is sufficient to overtake their PSF in the wings and they deviate strongly from the other three. Corrections, based on the bright stars, can be applied to these curves to obtain good estimates of their true brightnesses. The top panel presents growth curves as a function of normalized aperture sums while the bottom panel shows the curves as a function of magnitude differences within each successive aperture. The relative magnitudes of the point sources are given in the top panel and the image scale is the same as in Figure 5.6. From Howell (1989).

(those to be used in the differential measures) are extracted with the same (optimum) aperture and have identical PSFs. It is likely that on a given CCD image all stars of interest will not be of exactly the same brightness and will therefore not all have exactly the same optimum aperture radius (see Figure 5.7). Thus, a compromise is usually needed in which the extraction radius used for all sources of interest is set to that of the optimum size for the faintest stars. This procedure allows the faintest sources to produce their best possible S/N result while decreasing the S/N for bright stars only slightly. Another method is to use two or three different apertures (each best for 1/2 or 1/3 of the magnitude range) with the final differential light curves separated in halves or thirds by aperture radius (i.e., magnitude).

Advances in the technique of differential photometry have led to an output precision of 1 milli-magnitude for the brightest stars almost routinely. Everett and Howell (2001) outline the procedure in detail, providing the technique and equations to use and discuss a few "tricks" that help not only achieve very high precision but provide good results even for the faintest stars. The use of local ensembles of stars and production of an ensemble for every frame (not an average frame) are the main ones. Ensemble differential photometry is the method that provides the highest precision photometry one can obtain. This method will be used for the NASA Kepler Discovery mission to search for terrestrial size extra-solar planets, the GAIA Mission, and numerous ground-based time-resolved photometric surveys even in fairly crowded fields (e.g., Howell *et al.*, 2005; Tonry *et al.*, 2005)

5.5 Absolute versus differential photometry

Whether an observer needs to obtain absolute or differential photometric measurements depends on the objectives of the scientific and observational program. Absolute photometry results in a measurement of a given astronomical source leading to the true level of the flux received, say in ergs s^{-1}, or the total luminosity of a source in ergs, each within the specific band-pass used (e.g., a Johnson R filter). Differential photometry is just that: the final result is only known with respect to one or more other sources. This is a relative measurement, which, if the other source(s) are known in an absolute manner, can be placed on an absolute scale. All scientific measurements are really differential ones. The difference between absolute and differential measurements is simply that differencing from a known (in an absolute sense) source allows for an absolute result, whereas differencing from an unknown (in an absolute sense) source can only produce a relative result.

In photometric work one can view this in the following way. If the star Vega has its absolute flux known as a function of color (Tüg, White, & Lockwood, 1977), then a comparison of an unknown star with Vega would allow one to calibrate the unknown in an absolute sense. This differential measurement would produce an absolute result. However, if two unknown sources are compared over time, one may be seen to vary periodically allowing a scientific result to be produced, but its absolute flux is unknown. This is a differential measurement that produces only a relative result. If you are concerned about the true brightness of an object, say within a standard photometric system, or its color (e.g., B) in order to place it on an H–R diagram or to obtain its age or metallicity, then absolute photometry is needed. However, if you are after relative variability, say for periodicity analysis, or color indices (e.g., B–V) of a large group of stars such as a cluster in which you are looking for outliers, then differential photometry is likely to suffice.

A discussion of the observational and reduction techniques involved in absolute photometry is beyond the scope of this section. The reader is referred to any of the numerous books and articles that discuss the conversion of digital photometric data to (absolute) magnitudes and standard photometric systems (e.g., Hiltner (1962), Young (1974), Hendon & Kaitchuck (1982), Dacosta (1992)). The observational methodologies and equational transformations used to convert from CCD instrumental magnitudes to standard photometric system magnitudes are essentially identical to those used for similar observational programs with photomultiplier tubes (PMT). Absolute photometry from CCD data has been shown to be just as reliable and every bit as good as PMT measurements (Young, 1974; Walker, 1990; Kreidl, 1993). At the present, typical very good values for errors in the source magnitude for an *absolute* photometric result from CCD observations are $\pm 1\%$ or less.

Differential photometry concerns itself with the measurement of the difference in brightness of one or more astronomical sources when compared with one or more reference sources. With a two-dimensional CCD array, unlike the situation when using a PMT, it is often the case that multiple sources are imaged simultaneously and can therefore be used as references by which to compare the source(s) of interest. The assumption that is made in this simple approach is that the reference source(s) is not variable (at least over the time period of the observation) and the object(s) of interest can be compared with the reference source(s) on a frame-by-frame basis. The last step is important as it cancels out any seeing or atmospheric effects that may change with time.

The use of an ensemble of (bright) stars is common today when one is performing differential photometry. The brightest 20–50 stars in a CCD image (or a subregion of the CCD image) are averaged together, outliers

removed, and the averaging process performed again to convergence. Proper statistical use of each star in the ensemble as well as weighting the error contribution each makes to the ensemble is required. The ensemble value in each frame is then used as the reference to which all other sources are compared. This process continues on every frame in the time series and at the end light curves for every source are produced (e.g., Howell *et al.*, 2005). No "calibration" for an offset between CCD images is needed as the ensemble (of the same stars) in each frame sets the base level and by definition this level will be equal across frames.

To date, the effects of differential refraction, color terms, and seeing changes do not seem to pose an issue for properly implemented ensemble differential photometry. In fact, the level of precision being reached is near the limit of linearity of A/D converters and often reveals small changes in the CCD gain caused by thermal effects. Higher precision photometry would benefit from more stable CCD electronics and controllers in order to reach its full extent. Until then, be aware that at ultra-high precision, additional calibration work may be needed to correct the output magnitudes at the sub milli-magnitude level.

Proper statistical comparison of the object(s) of interest and the reference(s) must take into account all sources of error as well as photon statistics in order to use differential photometry correctly (Howell & Jacoby, 1986; Howell, Mitchell, & Warnock, 1988; Honeycutt, 1992; Howell, 1992; Everett & Howell, 2001). Differential techniques allow one to obtain incredible precisions from CCD data. For example, photometric errors of ± 0.001 magnitude are easily obtainable today with differential techniques (Gilliland *et al.*, 1993; Howell, 1993; Howell *et al.*, 1999; Howell, Everett, & Ousley, 1999; Everett *et al.*, 2002; and Howell *et al.*, 2005).

5.6 High speed photometry

Many years ago (about 30) in the dark ages of astronomical instrumentation, photomultiplier tubes (PMTs) were making their farewell to astronomy and with them went almost all of the studies of high-speed phemonena. The Universe is a fast-paced place and many sources change on time scales of less than 1 second. Accretion phenomena and rotation of neutron stars are a few examples. Studies of such events and other fast changes are being resurrected thanks both to a renewed interest and to CCDs and instruments that are capable of the task.

Today, there are only a few modern instruments that can observe the Universe in under 1 second. They come in two varieties; non-CCD instruments,

https://doi.org/10.1017/CBO9780511807909.007

which use avalanche photodiodes or PMTs, and 2-D digital cameras, which use frame transfer CCDs (such as UltraCam) or shutterless readout of OTC-CDs (such as in OPTIC). UltraCam (Dhillon & Marsh, 2001) can simultaneously obtain three-color imaging photometry with integration times (actually frame transfer times, which keep a reasonable noise level) of 1 second. Subsecond readout (down to a few ms) is possible for smaller regions of interest. OPTIC (Howell *et al.*, 2003) can perform shutterless readouts as short as 1 ms for up to four regions of interest simultaneously. New versions of OTCCDs being produced for the WIYN observatory will increase this capability to include essentially unlimited regions across the entire field of view. Some other examples of high-speed photometric applications are presented in Schwope *et al.* (2004) and Nather & Mukadam (2004).

High speed photometry is often used to study fast phenomena such as stellar eclipses or short period pulsations. It is also useful to obtain ultra-high

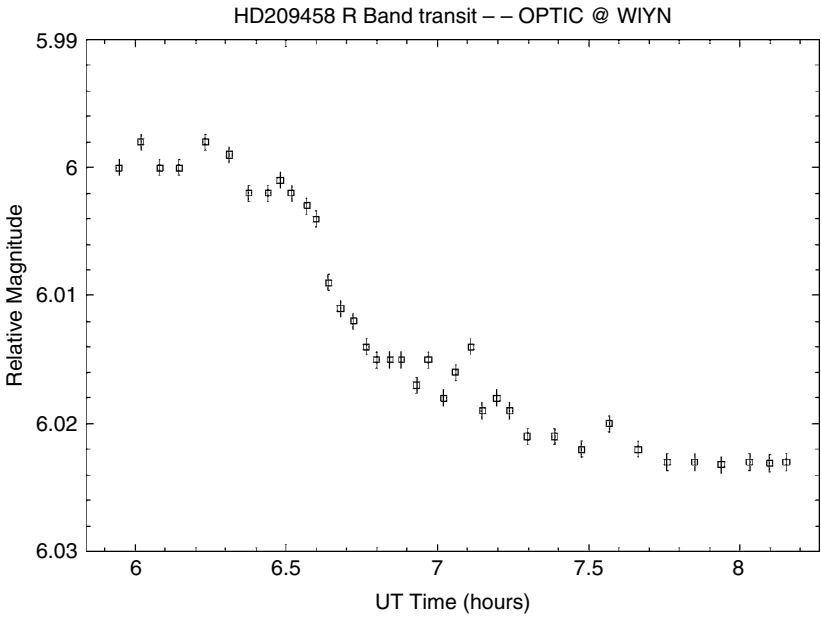

Fig. 5.9. Transit observation of the Jupiter-like extra-solar planet orbiting the V = 7.4 magnitude star HD209458. These R band photometric data were collected with the 3.5-m WIYN telescope using OPTIC and 1 ms integrations. Only the first half of the transit was measured as the observations were halted when the source reached an airmass of 2.5. Each CCD image collected over 10^6 photons and the time series has been co-added here to 58-s averages. The photometric precision per point is 0.0005 magnitudes. Data provided by the author.

precision photometry by allowing one to collect a large number of photons from (but not saturating) a bright source using rapid frame readout with later co-addition. Figure 5.9 illustrates this method as applied to the bright star HD209458, a G2V star with a Jupiter-like extra-solar planet. The planet transits the star every few days causing a $\sim$1.7% drop in its light. While the transit event itself is easy to observe, even for small telescopes, much of the detailed astronomical information needed to compare with models of extra-solar planet atmospheres comes from the ingress and egress shape of the transit and from measurements of the transit depth to high precision.

5.7 PSF shaped photometry

The theoretically best PSF shape for good photometric results is a top hat or mesa shape. Point sources, however, come in only one shape, round, and they approximate a Gaussian distribution when imaged on a CCD. This is not the case anymore! OTCCDs have the ability to shift their collected charge in the CCD during integration in order to provide tip-tilt corrections (see Chapter 2). This same feature can be put to use to manipulate the incoming photons into whatever shape the user desires in order to increase the output science. Howell *et al.* (2003) used this property of OTCCDs to produce square stars (Figure 5.10).

The photometric precision available with square stars is generally greater than with normal stars as the PSFs are better sampled and contain higher S/N for a given source magnitude. The shaped stars have none of the drawbacks of similar techniques (i.e., defocusing of bright stars) but do render faint background sources and 2-D objects (such as galaxies) unusable (Tonry *et al.*, 2005). One of the great benefits of PSF shaped photometry is its ability to greatly increase the high photometric precision dynamic range of a CCD. Figure 5.11 shows the relationship between the recorded magnitude of a source and the photometric precision of its light curve obtained with ensemble differential techniques. The panel on the left is a conventional CCD (with normal star images) and the right hand side shows a similar result for a PSF shaped data set obtained with an OTCCD. The solid line in the left hand panel is the theoretically expected result using the CCD S/N equation (Chapter 4). The difference in the two plots is obvious revealing that the PSF shaped result yields the highest photometric precision over nearly 5 magnitudes of dynamic range (Howell *et al.*, 2005).

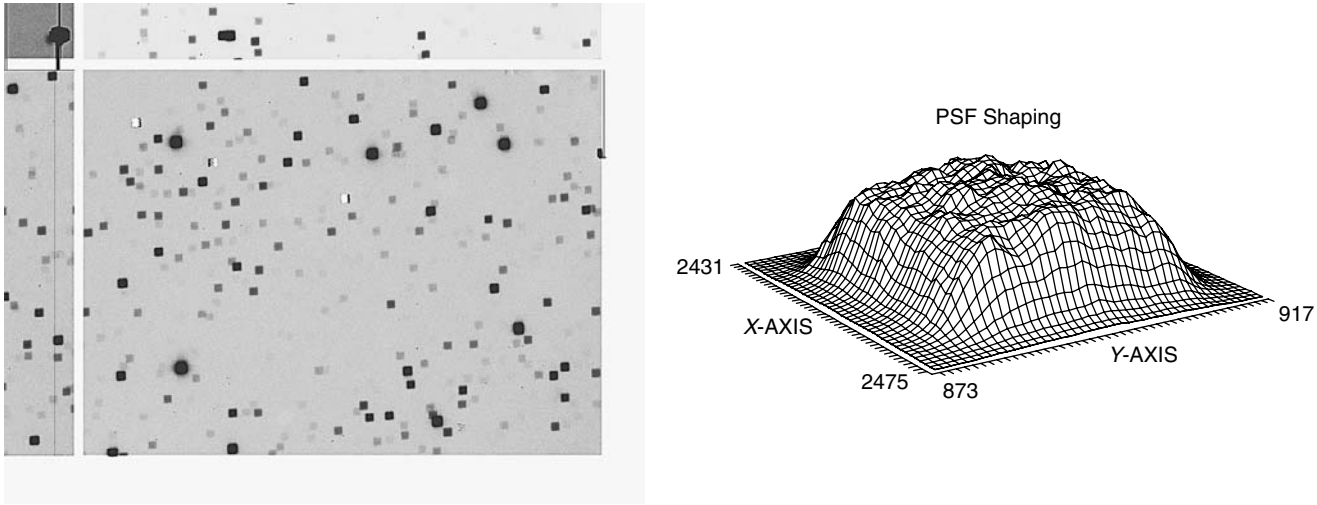

Fig. 5.10. PSF shaped star profiles using an OTCCD. The left hand panel shows a sub-section of an OTCCD image in which the stars were moved in a square shaped pattern (of 20×20 pixels) during each 300-second integration. The right hand panel shows a 3-D plot of one of the mesa-like PSFs.

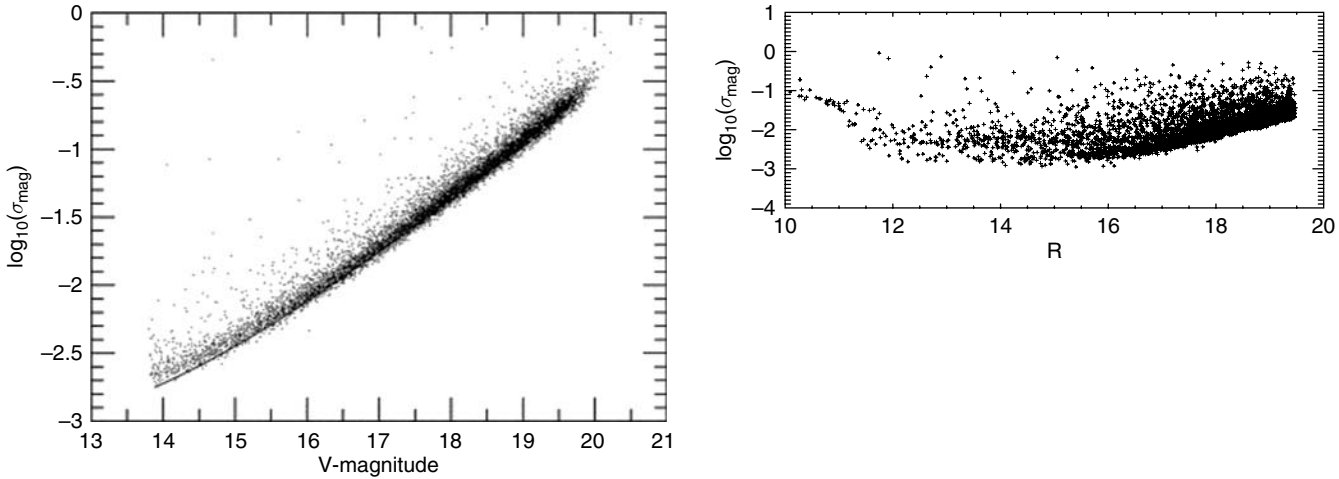

Fig. 5.11. Relationship between recorded stellar magnitude and the resulting photometric precision of the light curve for a sample of stars. The left panel is from a conventional CCD while the right panel is from an OTCCD using PSF shaping techniques. The shaped profiles (squares) provide similar high precision for about 5 magnitudes of brightness. Stars on the right, brighter than ~ 11, are saturated.

5.8 Astrometry

The science of the exact location and possible movement of astronomical sources has also been greatly advanced through the use of CCDs. Differential astrometric measurements of 1 milliarcsecond (mas) or better are achievable today, yielding new information on positions, proper motions, and parallaxes of astronomical objects. In differential astrometry, one measures the position of an object with respect to other objects within the same CCD field of view. This type of measurement is applicable to point source PSFs (e.g., stars) as well as moving objects (e.g., comets) and fuzzy objects (e.g., galaxies); however, the last two types of object have additional complexities not discussed here (Lasker *et al.*, 1990; Monet *et al.*, 1991; Monet, 1992).

Astrometric information is one method by which distance determination may be made for an object of interest. Of course the desire for a distance does not always translate into the ability to obtain such information. In general, in one night of obtaining a few good CCD observations, the determined position for a "well-behaved" star can be known to an astrometric accuracy of about 3 mas. A few tens of CCD frames taken over the course of a year (at a minimum of three different epochs) will allow astrometric accuracies near ± 1 mas to be reached, while the best astrometric positions to date have errors of ± 0.5 mas or less.

Astrometry performed with front-side illuminated CCDs will suffer from the effects of the overlying gate structures in ways such as we have discussed previously; that is, locating the exact center of the PSF is not without bias. The front-side gates must be traversed by incoming photons leading to a decreased (or no) blue response, intra-pixel variations in photometric (QE) response (Jorden, Deltorn, & Oates, 1994), and the need to use color terms to adjust the measured PSF centroid position to that of the actual source position. We will discuss an interesting CCD effect caused by intra-pixel QE variations in the next chapter.

Back-side illuminated CCDs present a different situation for astrometric work entirely. As mentioned earlier, their response to blue light is much improved and no major source of intra-pixel deviation exists. The physical flatness of a back-side illuminated CCD over its surface can be of concern and can introduce an additional term to be corrected for when measuring source positions and relative source offsets. Additionally, thinned CCDs may allow very long wavelength light to pass entirely through the device, be reflected back into the CCD itself, and be collected at a slightly different location (e.g., a neighboring pixel) from its original incoming path location. This long wavelength reflection effect can cause a slight blurring of the measured light

from the source, a particularly worrisome issue for astrometry of very late type stars. The best astrometric measurements to date, that is, the ones with the smallest rms error and greatest repeatability, have all been made with thinned, back-side illuminated CCDs.

As with any CCD imaging or photometric observation, the use of a particular type of CCD and filter combination will produce a different effective wavelength of the imaged scene and thus a change in the relative positions of different sources as a function of the zenith distance of the observation and the color (spectral type) of each individual source. There is no simple or even complete solution to this issue of differential color refraction but there are some items to note.[1] The use of narrow-band filters in front of your CCD is of help in this situation because such filters greatly restrict the band-pass of the observation, thereby reducing the effects of differential refraction and color terms. However, the use of narrow-band filters is usually impractical due to the large loss of incoming signal from the astronomical sources of interest. Astrometric observations made in long wavelength (red) band-passes have merit as they eliminate many of the refractive effects to start with. Finally, CCD observations obtained near source meridian passage are also a plus given that for an airmass of 1.0, refractive changes are essentially zero within the entire CCD field of view. Details of astrometric observations and a discussion of such effects is presented in Monet & Dahn (1983), Monet *et al.* (1991), and Girard *et al.* (2004).

Issues of related concern for precision astrometry involve image focus, seeing, use of different filters, PSF stability, telescope collimation, and many others (Monet, 1992). Detailed information concerning one's CCD is vital when attempting precision astrometry. For example, the standard pixel size value available in most of the literature for a 15-micron pixel TI CCD states that the pixel size is 15 microns across. However, the true pixel size is 15.24 microns, a difference of one quarter of a pixel, a value that can cause significant errors in precise astrometric measurements. Finally, even more subtle effects such as nonuniformly spaced pixels and improperly produced pixels that differ slightly ($\sim$1%) in size must be considered. A recent astrometric solution for the HST WFPC2 CCDs produces an accuracy to $\pm$0.1–0.2 pixels and appears to be limited here due to telescope breathing, variations across the filters, and even physical movement of the CCDs themselves (Anderson & King, 2003). The bottom line is, as in all cases where highly precise results are desired, one must know thy CCD in great detail.

[1] While reading the remainder of this paragraph, the reader may wish to skip ahead and glance at Table 6.2.

Data reduction methods of CCD images from which astrometric measures are to be obtained are similar to those discussed above for general CCD imagery. The differences in the process occur when the final reduced frames are to be used to produce output astrometric information. The interested reader is referred to the discussions and results given in Monet & Dahn (1983), Lasker *et al.* (1990), Monet *et al.* (1991), Monet (1992), and Girard *et al.* (2004).

5.9 Pixel sampling

An important consideration in photometric and astrometric measurements made with a CCD is how well the PSF is sampled on the two-dimensional array. PSFs that are well sampled by a CCD observation will lead directly to the result that the center and shape of the PSF will be known to higher precision, and thus one will obtain a final answer that will be of higher accuracy. We can define a sampling parameter, r, as follows (Howell *et al.*, 1996; Buonanno & Iannicola, 1989):

$$r = \frac{\text{FWHM}}{p},$$

where FWHM is the full-width half-maximum value of the source PSF and p is the pixel size, both values given in the same units. For r less than about 1.5, digital data are considered undersampled. As can be seen from the above expression, r will be small for the case of a CCD with large pixel sizes compared with the total areal coverage of the imaged PSF. The other possible case of small r values is if the CCD image contains very tight PSFs such as those that might be obtained at observing sites with very good seeing, if using adaptive optics systems, or for CCD images obtained outside the Earth's atmosphere (i.e., space-based telescopes). Real life examples of cases that will produce undersampled images (i.e., small r values) are a typical wide-field telescope outfitted with a large-format CCD, such as a Schmidt telescope or a camera lens, or a space-based telescope such as the Hubble Space Telescope wide-field planetary camera (WFPC) (Holtzman, 1990; Howell *et al.*, 1996, and Section 7.1).

Anytime the value of r approaches the limiting case of undersampling, standard software methods and techniques of astrometric and photometric data analysis will begin to produce increasingly larger errors and poorer fits as r decreases further (see Section 7.1). Photometric and astrometric errors obtained from CCD observations are related in that the analysis techniques for

each type of measurement are very similar. Both photometry and astrometry require intimate knowledge of the centroid position of the source PSF. However, it has been shown (King, 1983; Stone, 1989; Howell & Merline, 1991) that for undersampled data the photometric error is least for source PSFs

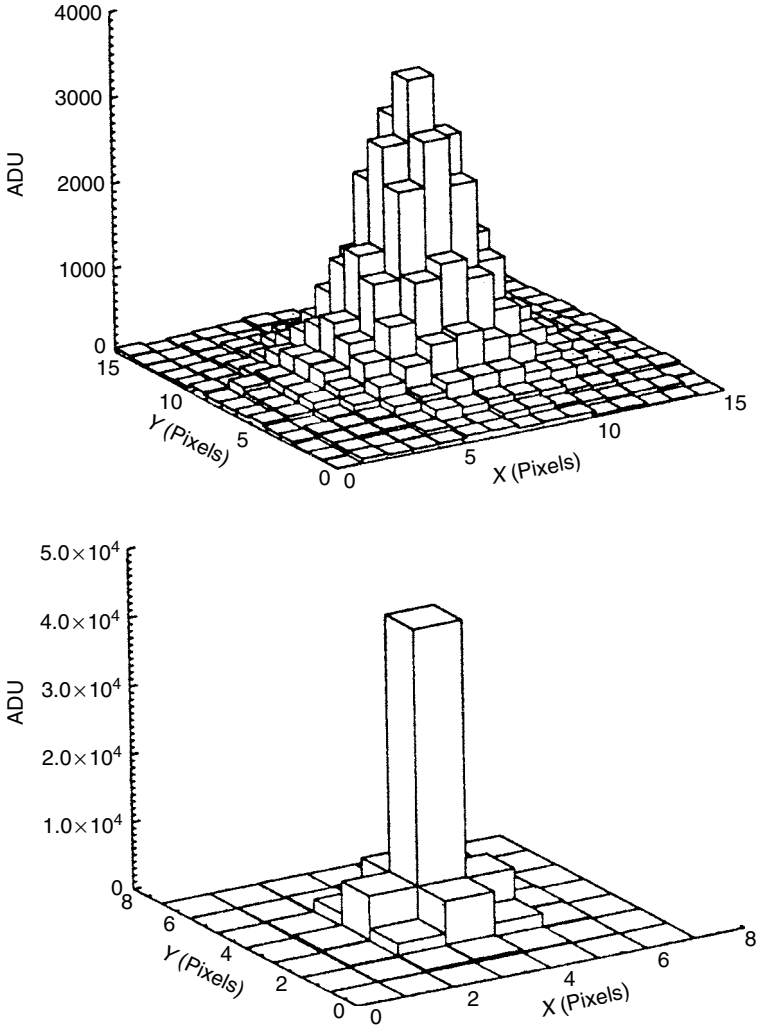

Fig. 5.12. The effects of pixel sampling are shown. The top PSF is a well-sampled star image with a S/N of near 230. The bottom panel shows the same PSF but now severely undersampled and centered at the middle of a pixel and (next page) at the corner of four pixels respectively. Note that the undersampled profiles are not well represented by a Gaussian function. From Howell *et al.* (1996).

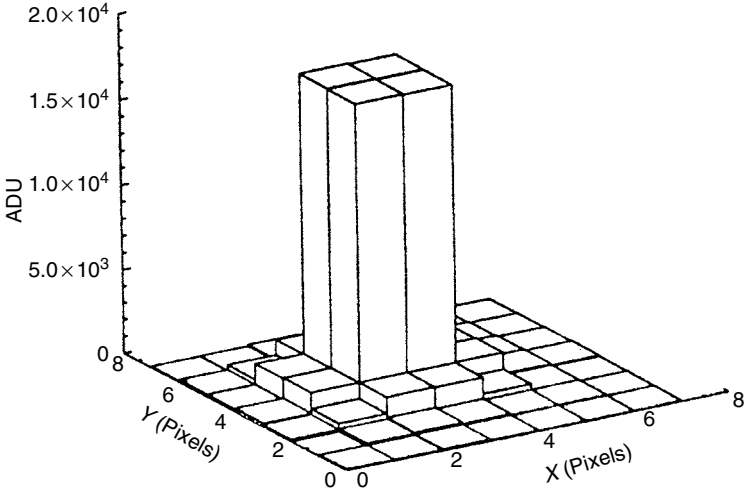

Fig. 5.12 (cont.)

that are centered on the edge of a pixel or exactly at its center, whereas for astrometric data, the resulting error is least when the source PSF is centered midway between a pixel's edge and its center.

The rule of thumb for pixel sampling on a CCD follows directly from the statistical result of Nyquist sampling. That is, sampling of the PSF of an astronomical source will be optimal in terms of S/N, error rejection, data analysis, and so on for a source PSF that has its FWHM value sampled over about two pixels (i.e., FWHM $\sim 2 \cdot$ pixel size). For example, if the average seeing at an observing site produces source PSFs with FWHM values of 2 arcsec, then an ideal (optimal) CCD pixel size to use would be one for which each pixel within the array has a projected image size of 1 arcsec across.[1] A rigorous mathematical definition of undersampling, based on the Nyquist theorem, identifies critical sampling as the sampling interval that is equal to the width (i.e., standard deviation) of the PSF. For a Gaussian PSF this corresponds to a FHWM equal to 2.355 pixels. Of course an ideal image scale is hard to meet in reality as seeing and telescope focus change with time, source PSFs generally do not fall onto the CCD pixel grid exactly on a pixel boundary, and one generally has only a limited number of available CCD cameras with fixed pixel sizes.

[1] The determination and measurement of CCD pixel size or plate scale was discussed in Section 4.1.

Since CCD detectors do indeed sample astronomical sources in a quantized manner, pixel sampling within the array will cause even identical PSFs to change their detailed appearance slightly, even within the same observation. The effects of such sampling differences become worse as the sampling parameter (r) becomes smaller (Howell & Merline, 1991; Merline & Howell, 1995). Figure 5.12 illustrates some examples of various values of r caused by CCD pixel size. The top panel shows a well-sampled source PSF that appears to be more or less Gaussian in shape. The remaining two panels in Figure 5.12 show the same model PSF but now imaged as a poorly sampled ($r = 1$) source. The undersampled cases are for a source PSF with a pixel-centered centroid and a corner-centered centroid respectively. Notice in Figure 5.12 that the undersampled PSFs are not well represented by a Gaussian function (Buonanno & Iannicola, 1989; Holtzman, 1990; Howell & Merline, 1991; Howell *et al.*, 1996).

5.10 Exercises

1. How do the numbers in Table 5.1 help us understand the fact that the sun appears red at sunrise and sunset?
2. At what wavelength would you choose to observe an astronomical source if you could only point your telescope at an elevation of 20 degrees?
3. Describe in words what a point-spread function is. Do extended objects, such as galaxies, have PSF's? If they do, what do they look like?
4. Write a computer program to find the center of an astronomical image that has a circular shape (and radial light profile) when projected on a 2-D surface. Try various techniques and determine: which centering method is the fastest? Which is the best? What if the shape were triangular? A square?
5. Write a computer program to calculate the PSF of a star imaged on a CCD. Use the information in the previous chapter to include all noises in the calculation.
6. Using Figure 5.2, describe the need for a star aperture, a background annulus, and why they are circular. Would other shapes work as well?
7. Perform a qualitative analysis of why, or why not, partial pixels are important in stellar photometry. How does your answer relate to the CCD pixel size and plate scale?
8. Using the results presented in Figure 5.3, discuss quantitatively the error term $(1 + n_{pix}/n_B)^{1/2}$. This term was introduced in Chapter 4.
9. Read the paper by Tüg *et al.* (1977). What is so important about the star Vega? Can you design a similar experiment to try with your CCD camera?

10. Make plots of each of the model PSFs (given as equational representations in Section 5.2). How do they compare to the PSFs shown in Figure 5.4 and those in Diego (1985) and King (1971)? How do the pixel scale, plate scale, and plot type influence your answer?
11. Why is the FWHM of a PSF an important (dimensionless) value? What is so special about the value $3 \cdot \text{FWHM}$? Explore the parameters "encircled energy" and "Strehl ratio" and relate them to the FWHM of a PSF. Which is a better descriptor of a PSF?
12. Discuss why PSF fitting photometry is the best method to use for the determination of absolute photometry of a source.
13. Make a table of pros and cons for PSF fitting, DIA, and aperture photometry. Which of these are differential measurements? Which are absolute? Discuss which is best to use for the following observational projects: Stellar photometry of variables in the LMC, supernovae searches in external galaxy clusters, light curve observations of a 20th magnitude star, and making a color magnitude diagram for an open cluster.
14. Determine the faintest source for which one can achieve a S/N of 50 in a photometric measurement lasting 1 second. Assume the image was obtained with a typical LBL CCD in the R band and used a 3.5-m telescope. Can you determine a simple relationship between telescope aperture, source brightness, and integration time for a given S/N?
15. Prove that a square star (top hat) profile provides the best S/N for a point source. What type of PSF shaping might be useful for extended object photometry?
16. At the current best limit of CCD astrometry, what is the furthest distance at which a star can be and still have its parallax measured?
17. Design an astrometric observational program that would provide ideal results for a sample of very blue objects. Discuss the type of CCD, telescope, and filters you would use. What if the program sample were red sources?
18. Discuss how different pixel sampling (over-sampled and under-sampled) would affect photometric observations with a CCD. Be specific for the methods of PSF fitting, DIA, and aperture photometry. How do these same parameters affect spectroscopic observations with a CCD? (Hint: if you get stuck here, read ahead to Chapter 6.)